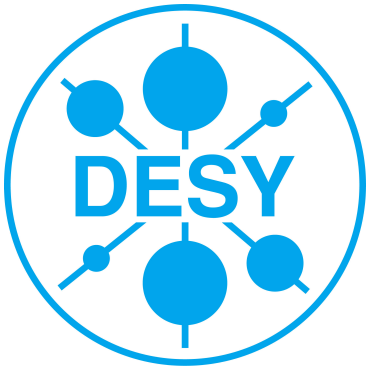

Summer students programme final report

Performance analysis of diamond sensors desined for BCM1F

Jerzy Mańczak, University of Warsaw, Poland

supervised by
Roberval Walsh

September 7, 2016

Abstract

The paper presents single crystalline diamond sensors efficiency analysis with the data collected from BCM1F detector during the current(2016) LHC run. The analysis shows that after around 20 fb^{-1} the diamond sensors suffered significant efficiency loss due to radiation damage and therefore now it is necessary to replace them. Also first results from performance tests of different kinds of possible future diamond sensors for BCM1F are shown. The results show better performance of single crystalline diamonds compared with polycrystalline.

Contents

1 Introduction

BCM1F (Fast Beam Condition Monitor) detector is a part of a BRIL system (Beam Radiation Instrumentation and Luminosity), which was designed for monitoring beam conditions inside CMS (Compact Muon Solenoid) detector to prevent CMS components from damage caused by unexpected beam loses. BCM1F is installed close to the IP (Interaction Point). Originally it was meant to diagnose very fast changes in beam conditions close to the CMS tracker to prevent it from potential damage [1]. Currently BCM1F operates as a luminometer of CMS detector and provides information about machine induced background. Because of requirements of these tasks, BCM1F offers time resolution at the nanoseconds level which allows it to distinguish collision products from background events. So far it was using single crystalline diamonds as sensors material. After long time of successful operating it is time to consider sensor replacement due to damage caused by very high radiation environment and future luminosity increase in LHC.

2 Diamond as a particle detector material

Diamond as the material for particle physics detector is known for it's fast response time and very good radiation hardness. Moreover, it doesn't need an additional cooling and can sufficiently work at room temperature. Also the temperature dependence of leakage current is negligible. All of these features makes diamond very appropriate for BCM1F applications and it's exposure to strong radiation due to close distance to interaction point. The time resolution of several nanoseconds allows to discriminate signal from beam halo and collision products. Two different types of diamonds are already installed and operating well in BRIL system, polycrystalline pCVD and single crystalline sCVD. CVD acronym corresponds to Chemical Vapor Deposition, which names the diamond production method. Now both of these types are taken into account in terms of future sensor exchange in BCM1F detector. In general polycrystalline diamonds are expected to be even more radiation hard than sCVD, but they provide a lot worse signal. The valence band gap in diamond equals 5.23 eV and the mean number of electron-hole pairs generated by MIP (Minimum Ionizing Particle) crossing the diamond equals to $36/\mu$m [3].

3 BCM1F detector

During the current LHC run BCM1F detector operates with 24 sCVD single crystalline diamond sensors (5x5x0.5 mm), 12 per each side of the IP. The sensors are attached to 4 C-shaped half rings at 1.83 m distance from each side of IP. They are installed radially at a radius 7.2 cm from the beam axis [5]. Every diamond sensor has two separately metalized channels. Figure 1 shows BCM1F position inside the CMS. When the charged particle crosses the diamond, it produces electron-hole pairs, which drift to the electrodes. Then the signal is amplified and converted into an optical signal by the FEE (Front-End Electronics). After transmission through optical fibers, the signal is converted again into electric by optical receiver and can be further processed by Back-End Electronics. Before

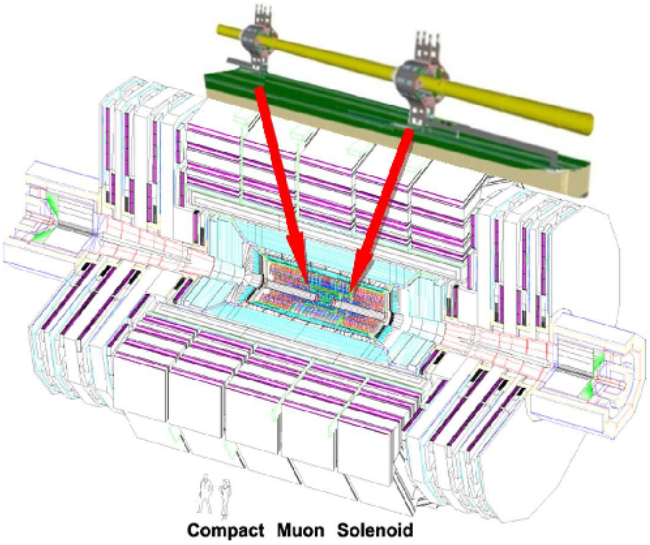

Figure 1: Position of BCM1F detector inside CMS. On both sides of IP sensor rings in carbon fiber cases are shown.

Source: *Fast beam conditions monitor BCM1F for the CMS experiment* [1]

going to other components of BEE, the signals are split into an ADC and a discriminator, after which the signals are counted in the RHU.

3.1 Sensors

So far BM1F was using 24 single crystalline diamonds (sCVD) with dimensions 5x5x0.5 mm. Each diamond has a two pad metalization separated by 25 μm gap. This configuration leads to 48 readout channels divided equally for each side of IP.

3.2 Front-End Electronics

A dedicated front-end ASIC (Application Specific Integrated Circuit) allows to fully distinguish pulses with from hits separated at a time of 12.5 ns. The time resolution can be improved up to 10 ns with signal processing methods. Peaking time, depending on the specific configuration can vary from 6.6 to 9.6 ns and the full-width-half-maximum of the pulse is around 9 ns [5]. These time intervals do no depend on the pulse height. Linearity of the output voltage created by the input charge can be achieved up to 9 fC, which exceeds any of real measured signals.

3.3 Back-End Electronics

The Back-End Electronics module consists of few different devices:

- ADC - The ADC has 8 separate channels with 2 ns sampling time. The memory buffer allows to store data from 4 ms time length. ADC produces binary output in

units of ADC counts from the electric signal produced by charged particle crossing the sensor. One ACD count corresponds to 4 mV of analogue signal.

- Discriminator - It generates standard output rectangular pulse for each sensor signal above the given threshold. The threshold can be set individually for every channel and it is set to suppress the electric noise of each channel.
- RHU - Real time Histogramic Unit processing signals in real time and creates histograms of their's amplitude.

4 Sensors efficiency analysis

Using the data collected by the RHU from BCM1F during current LHC run an efficiency downgrade of sCVD diamonds was investigated. For the purpose of that research the best performing channels were chosen. These channels (40,41,44 and 45, located at -Z side of IP) were used for the background and luminosity measurement, because of their's clean signal and good high voltage stability. Some data was also taken from channels 3, 8, 12, 15 (located at +Z side of IP) and 32, which performed a little worse than the lumi channels, but were still used for background measurement. Locating the background channels on both sides of the IP is important due to beam halo measurements for both colliding beams. All of the investigated LHC fills were performed in a short time after the Vad der Meer scan [4], so one assumed that the colliding beams profile didn't change during these fills. While investigating a specific fill, only the first bunch in each train was taken for the rate calculation. As it is shown on the Figure 2, the rates of crossing particles doesn't come down immediately after the end of a train. The method meant to always choose the "cleanest" bunch from each train for analysis. Rates measured by each channel were normalized by the product of bunch intensities. Concerning the formula:

$$\sigma = \frac{R\Sigma_x\Sigma_y}{N_1 N_2},$$

where

- σ is inelastic crossection,
- R is a measured rate,
- N_1 and N_2 are colliding bunches intensities,
- Σ_x and Σ_y are bunch horizontal and vertical beam widths,

and the above assumption, the normalized rates should not change during the time of measurement. Figure 3 shows the plot of measured rates for several fills fitted with a constant. Just by looking at the plot from Figure 3 it becomes obvious that efficiency of the sensors decreases with the increasing fill number or accumulated integrated luminosity. On Figure 3, for fill no. 5029, the polarization effect is clearly visible. The polarization effect is related to short time efficiency recovery caused by flushing charge traps created by

radiation damage. These traps, during normal sensor operating, get filled with charge and change electric field inside the sensor. If there is enough time between fills, at least some of the trapped charge can escape and restore previous performance. It was noticed that polarization effect is constantly growing with amount of radiation taken by the sensor, but then it just disappears and some kind of "saw tooth" shape of efficiency shows up (fill no. 5117). This new effect may be caused by very fast polarization, which can take place even in short time between trains. However that "saw" shape effect needs further research. Figure 4 shows relative efficiency for all of the investigated fills. Long term hyperbolic behavior of efficiency is expected and this assumption seems to be consistent with the results shown on Figure 4. Because of the efficiency degradation change of the sensors will be necessary for the future BCM1F operation. On figures 5, 6, 7 and 8 efficiency downgrades for specific channels are shown. It is understandable that performance of different channels may vary, but as it is shown on figures 5 and 6 performance of channels may vary even if they are on the same diamond. That behavior may be explained by heterogeneous distribution of defects inside one diamond.

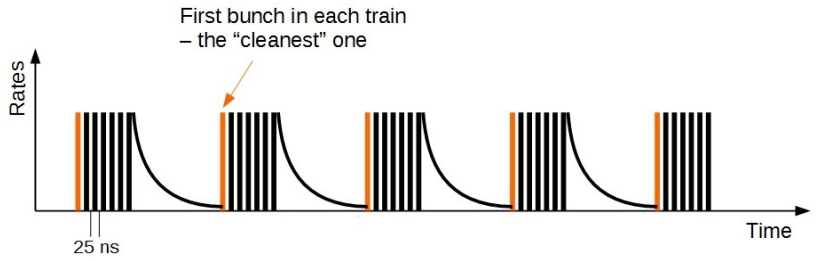

Figure 2: Sketch of the LHC filling scheme

5 Test beam results analysis

The test beam for analysis of pCVD and sCVD diamonds was performed in T9 beam line at CERN. All kinds of available particles were used: muons, electrons, hadrons and pions with energies in range 1-15 GeV. Threshold applied for peak finding algorithm during the data analysis was set on 4 ADC counts for all investigated configurations of both types of diamonds. In analyzed data channel 1 corresponded to one metalization pad on pCVD diamond and channels 2 and 3 were connected to separate pads on the same sCVD diamond. Figure 9 shows an example raw ADC data. As the sensors performance criteria charge collection distance (CCD) and signal to noise ratio were posited. Signal to noise ratio is simply defined as MPV (Most Probable Value) of measured particle energy divided by the RMS (Root mean squared) of noise distribution [2]. In that case energy was expressed by corresponding signal amplitude. The noise distribution from example configuration is shown Figure 10. Usually charge collection distance value corresponds to the mean CCD which is calculated by taking mean value of measured energy distribution converted to number of collected electrons and dividing it by number of electrons generated by MIP on path unit. Since for the expected convoluted Landau+Gaussian [2]

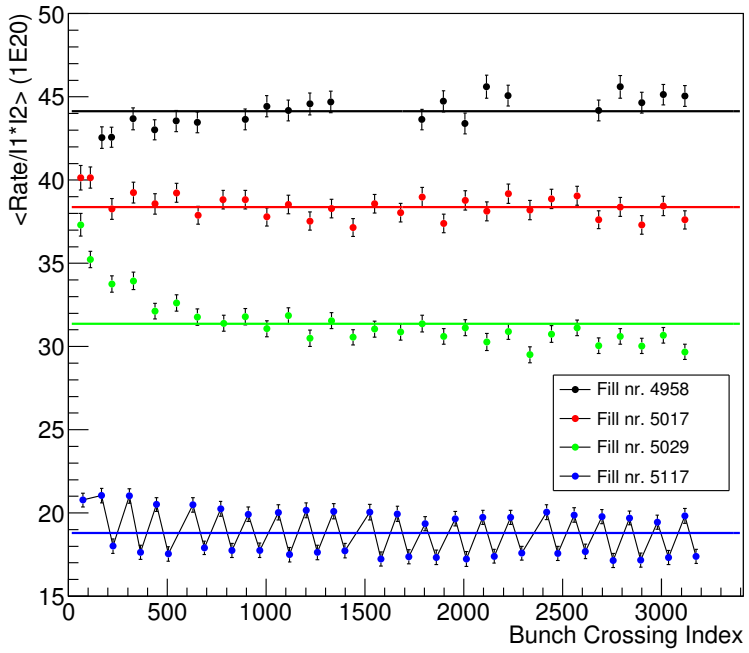

Figure 3: Measured summed rates from luminosity channels divided by the product of bunch intensities for some example fills. Each point represents first bunch in a train.

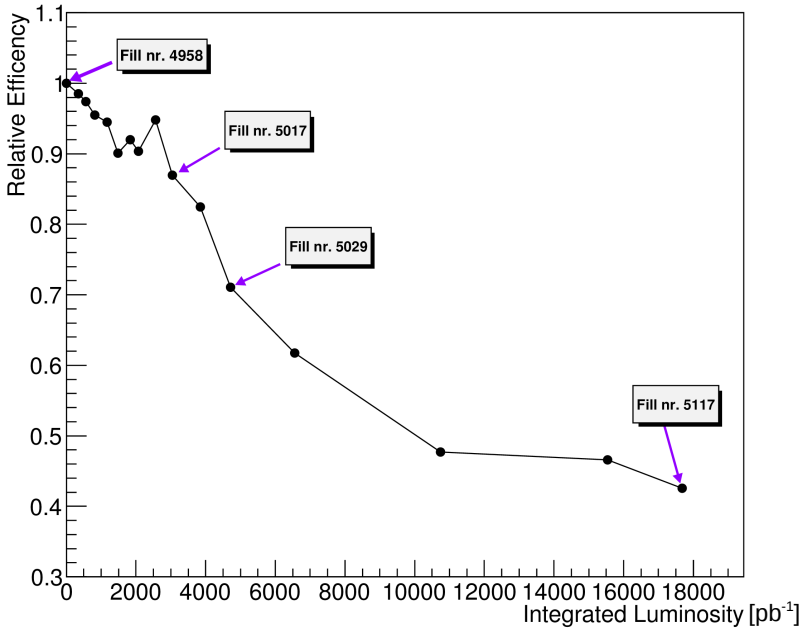

Figure 4: Summed rates from the luminosity channels normilized by the product of bunch intensities. Efficiency degradation of the sensors is noticeable

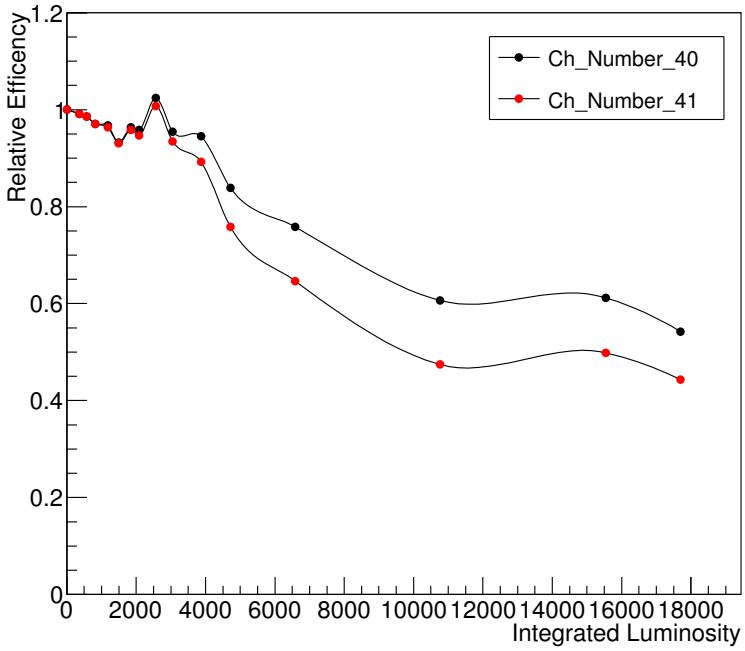

Figure 5: Efficiency of separate channels of the first luminosity diamond sensor

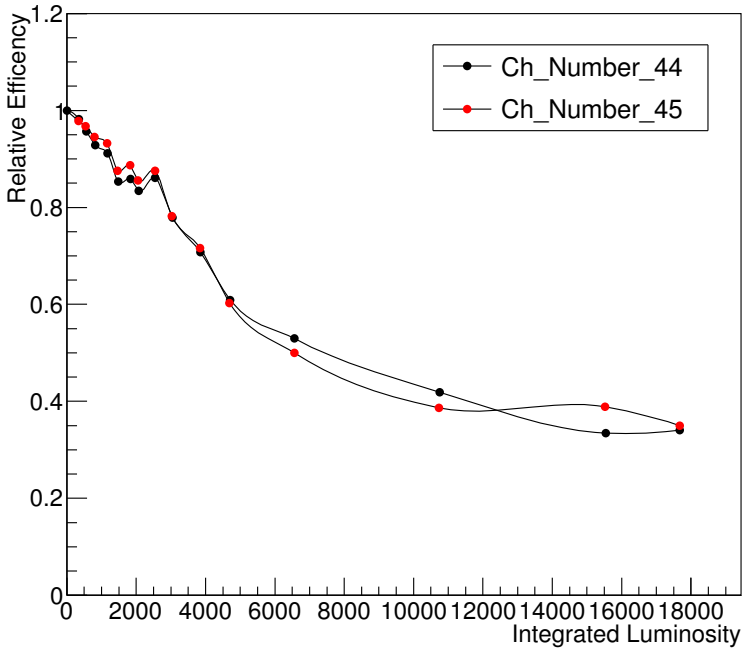

Figure 6: Efficiency of separate channels of the second luminosity diamond sensor

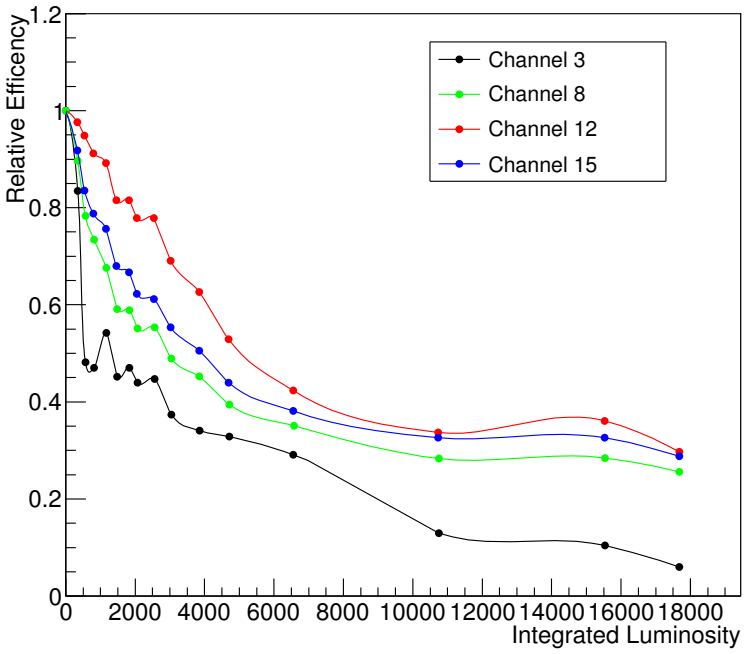

Figure 7: Efficiency of background measurement channels

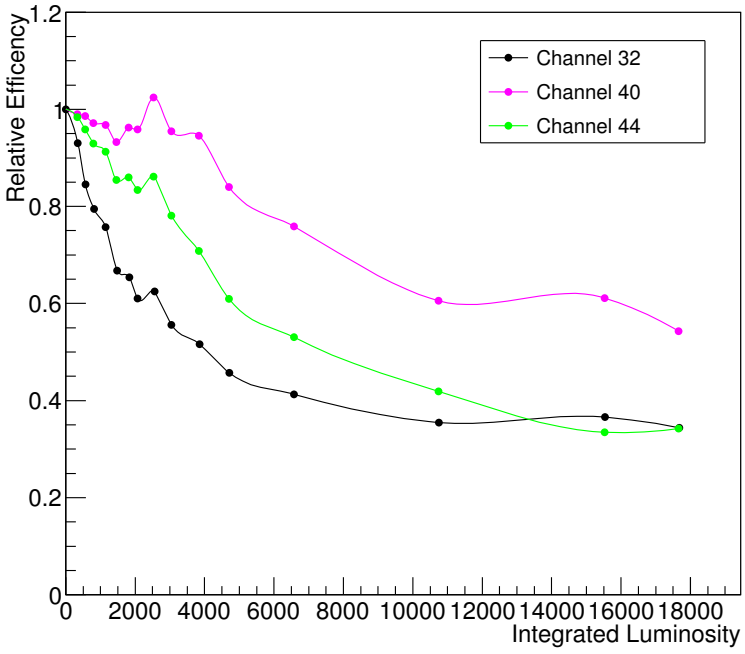

Figure 8: Efficiency of one of the background measurement channels compared with luminosty channels

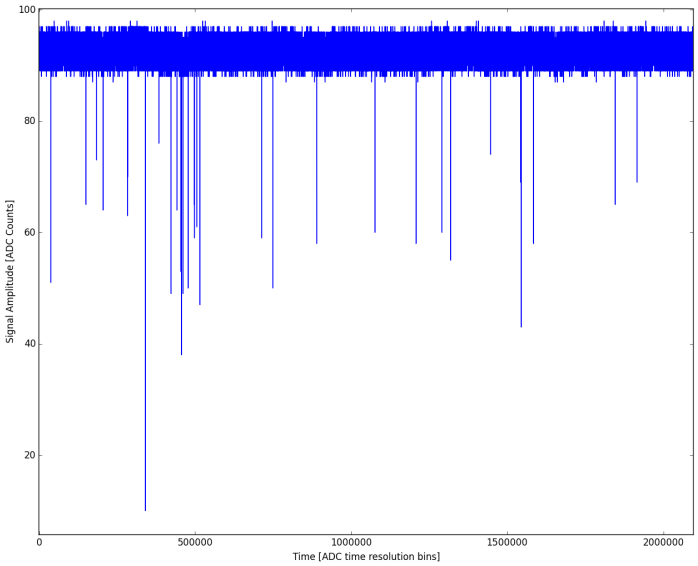

Figure 9: An example of raw ADC data from signle crystalline diamond

distribution of signal peak mean value is not defined, the MPV value was taken for CCD calculations instead of mean. However, the exact values did not matter that much for purpose of this analysis because it's main goal was to do rather qualitative comparison of different configurations.

5.1 Single crystalline diamonds

Single crystalline diamonds tests were based only on the bias voltage scan. Roughly estimated signal-charge calibration factors for channels 2 and 3 were equal to η_{ch2}=0,0828 fC/mV, η_{ch3}=0,0706 fC/mV. For all amplitude histograms from sCVD diamonds a convoluted Landau+Gaussian fit with chi squared optimization was performed, but only in range of the signal peak since it (the signal peak) was always very well separated from noise pedestal. Figures 11, 12, 13, 14, 15, 16, 17, 18, 19, 20, 21 and 22 show data from single crystalline sensors analysis. The maximum value of y axis on histograms was fixed on 1000 counts to get a better view on the signal peaks. Figure 23 shows whole amplitude distribution for example configuration. Optimization was based on changing the minimum value of the fit in range from 25 to 35 ADC counts with fixed maximum on 80 ADC counts. The exclusion of the tail visible on the left side of each signal peak was done on purpose, because it was already investigated that it could be caused by the efficiency drop on the edges of metalization pad [2]. Figure 24 shows CCD calculated for both channels of sCVD diamond and Figure 25 shows signal to noise ratio. It can be seen that behavior of these channels is slightly different even though they were taking data from the same diamond. The most probable reason for that is different front-end electronic configuration, which for example changes the signal-charge calibration. Saturation of CCD is clearly noticeable for both channels. Signal to noise ratio for channel

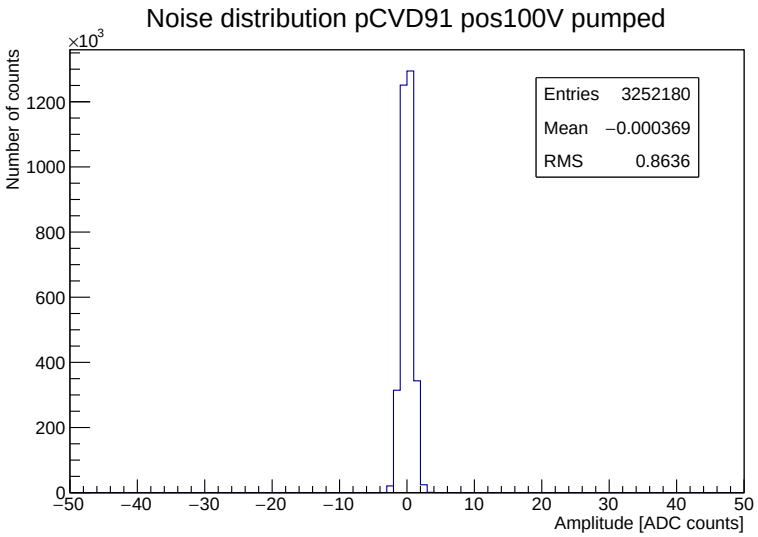

Figure 10: Noise amplitude data from pCVD91 pos1000V pupmped configuration relative to the baseline value

3 fits very well in CCD shape, but for channel 2 saturation is no longer visible. That difference was caused by behavior of noise, which can be seen on figures 26 and 27. It is not expected for noise to change with bias voltage increase, so the noise results need to be deeper investigated in terms of apparatus configurations. All calculated values of CCD and SN ratio for sCVD are shown in Table 1.

5.2 Polycrystalline diamonds

It was found that for the best results in poly crystal analysis, particle hit signals should be triggered by signals also found in channel 3. Signal-charge calibration factor was calculated more precise and it can be described by function Q=-6.602·ln(1-0.001·U), where Q is charge in fC and U is signal in ADC counts. Amplitude data from all investigated pCVD configurations can be found on figures 28, 29, 30, 31, 32, 33, 34, 35, 36 and 37. For the configurations in which a signal peak was unable to distinguish no fit was performed. However, even for the configurations with distinguishable signal peak, a certain part of the peak was covered by the noise pedestal. That situation made impossible to find one distribution which could describe well all of the pCVD data. It was found that two functions, Vavilov or summed Landau-gaussian+Gaussian can provide reasonable results. The amplitude spectra of best performing pCVD configurations were fitted with one of these functions depending on the most adequate distribution shape. For one configuration, shown on Figure 36, MPV peak value was found manually since none of fit functions seemed to work well with this configuration data.

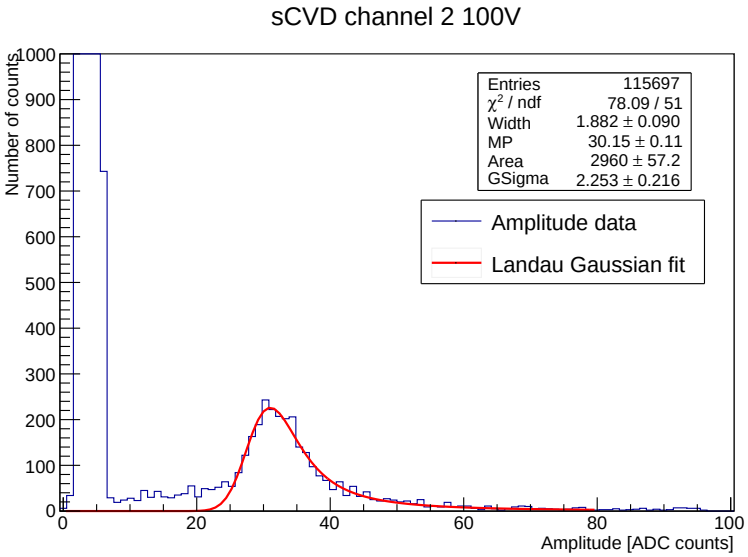

Figure 11: Amplitude distribution for sCVD channel 2, 100V bias voltage

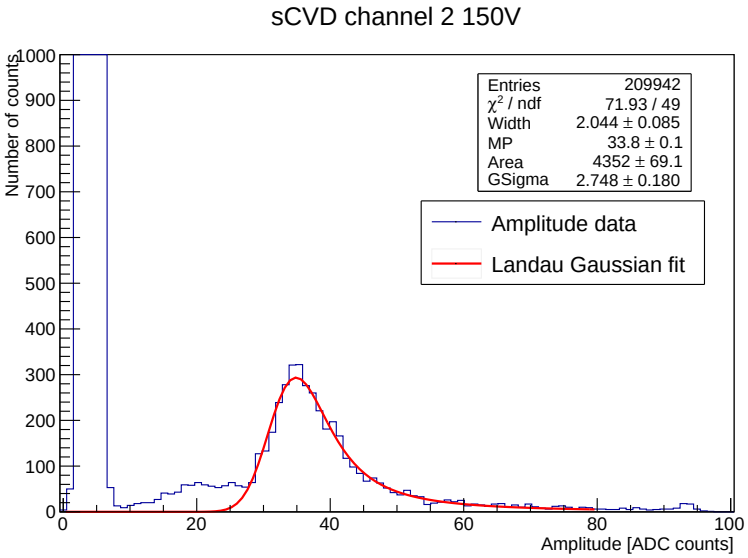

Figure 12: Amplitude distribution for sCVD channel 2, 150V bias voltage

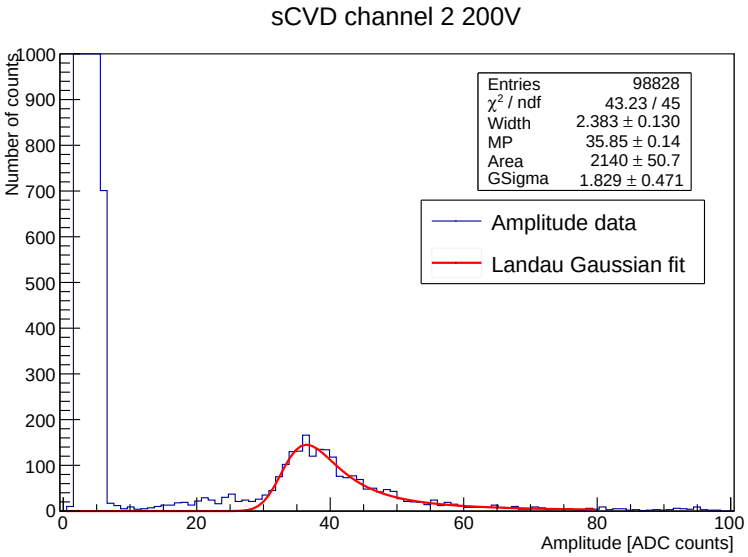

Figure 13: Amplitude distribution for sCVD channel 2, 200V bias voltage

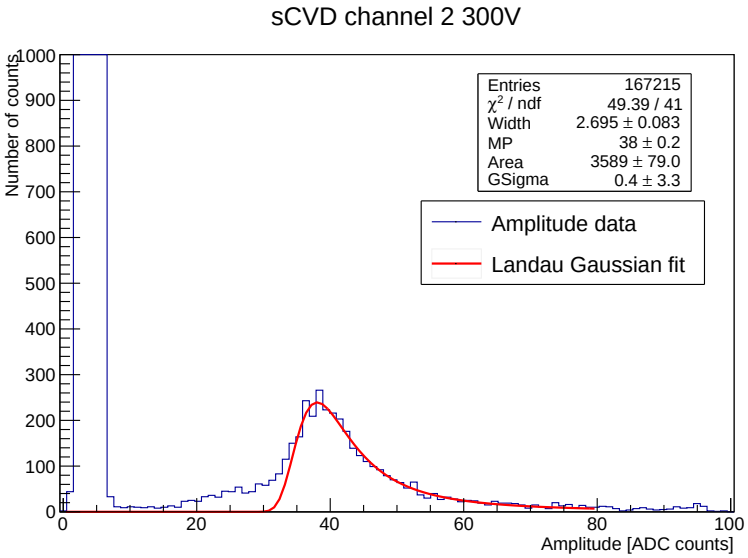

Figure 14: Amplitude distribution for sCVD channel 2, 300V bias voltage

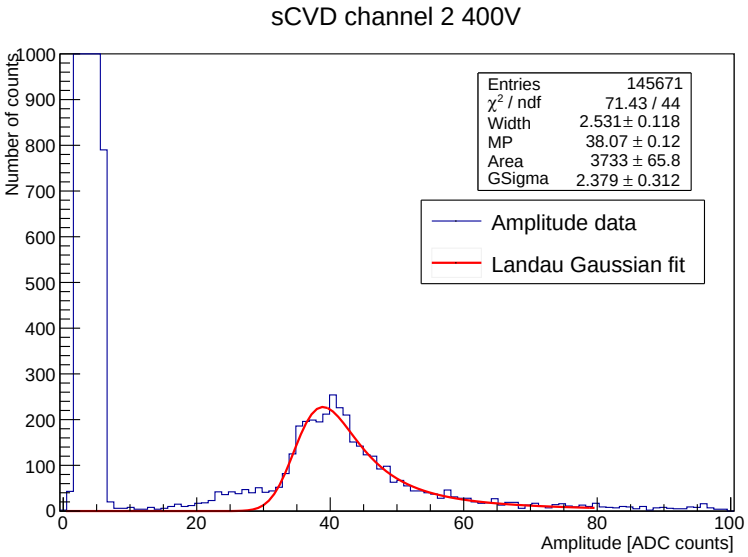

Figure 15: Amplitude distribution for sCVD channel 2, 400V bias voltage

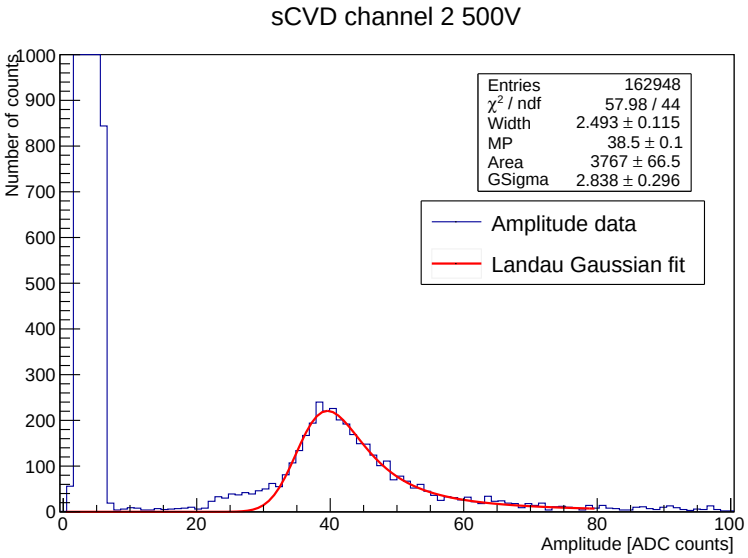

Figure 16: Amplitude distribution for sCVD channel 2, 500V bias voltage

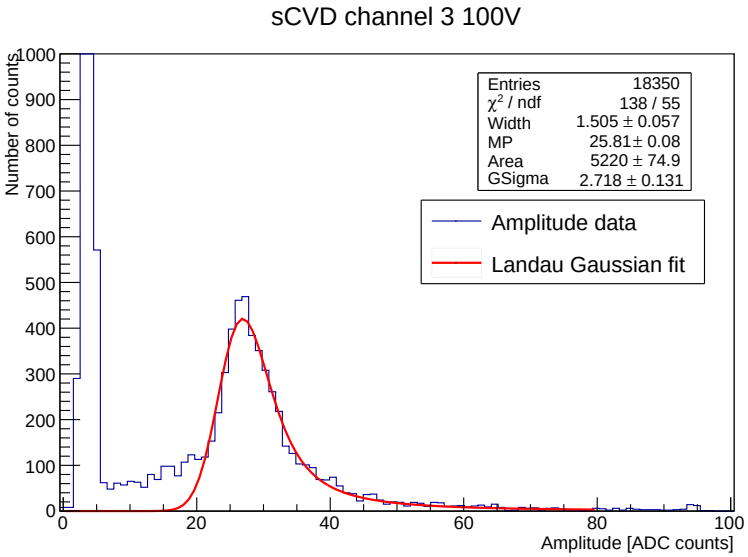

Figure 17: Amplitude distribution for sCVD channel 3, 100V bias voltage

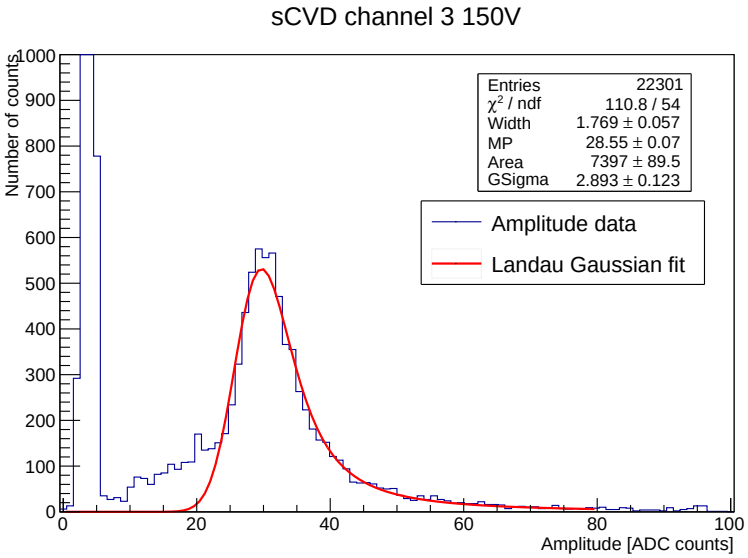

Figure 18: Amplitude distribution for sCVD channel 3, 150V bias voltage

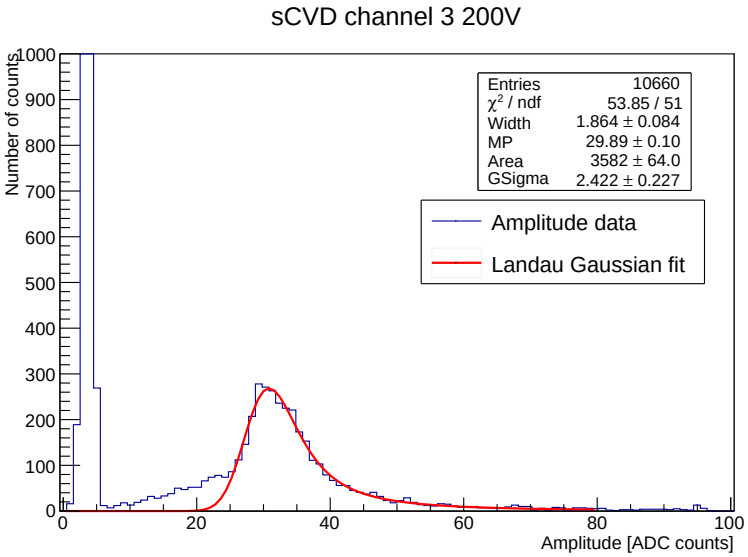

Figure 19: Amplitude distribution for sCVD channel 3, 200V bias voltage

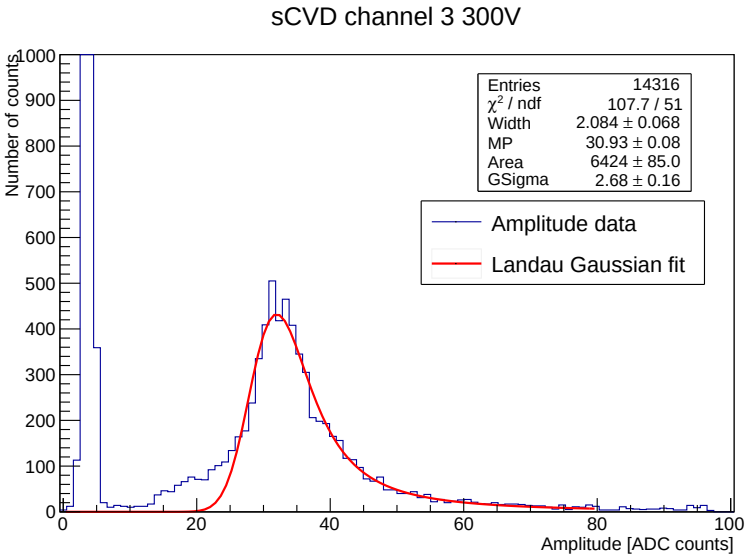

Figure 20: Amplitude distribution for sCVD channel 3, 300V bias voltage

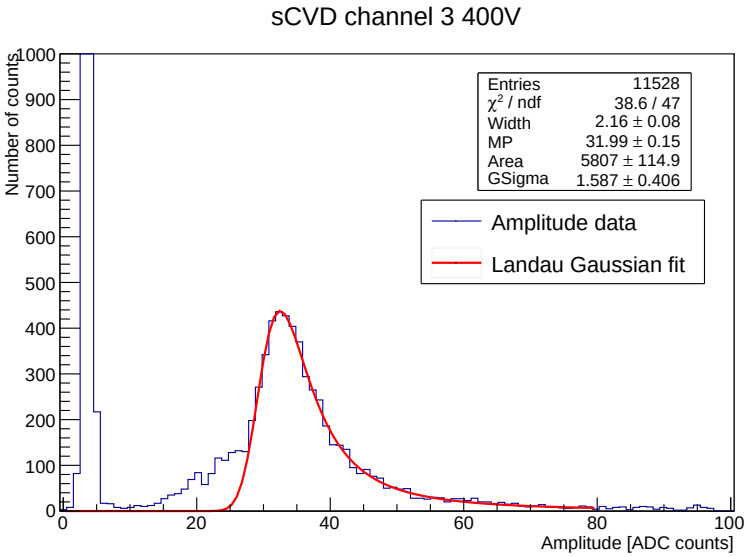

Figure 21: Amplitude distribution for sCVD channel 3, 400V bias voltage

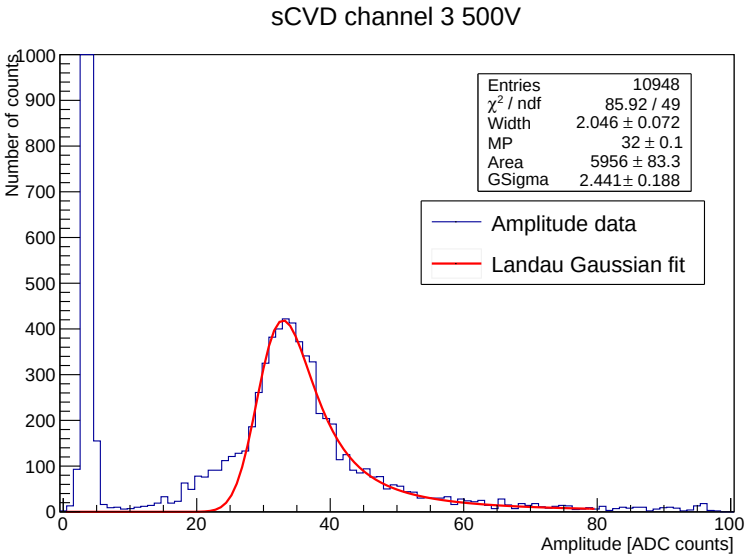

Figure 22: Amplitude distribution for sCVD channel 3, 500V bias voltage

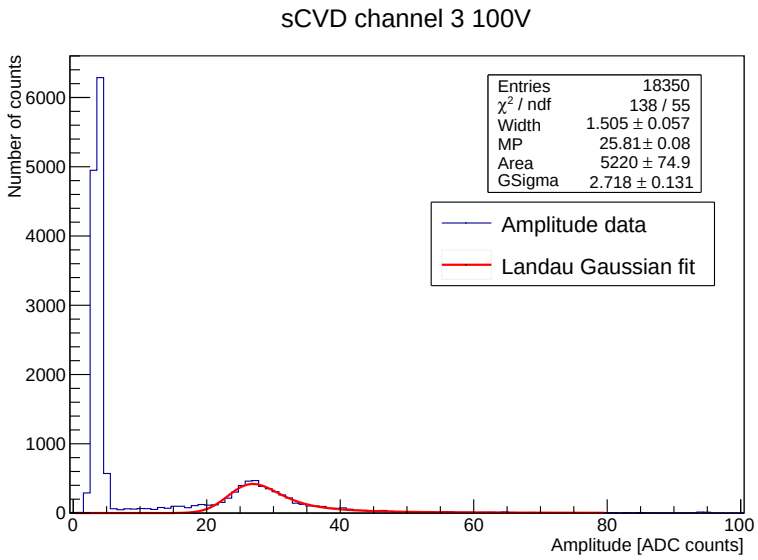

Figure 23: Whole amplitude distribution for example configuration of sCVD sensor

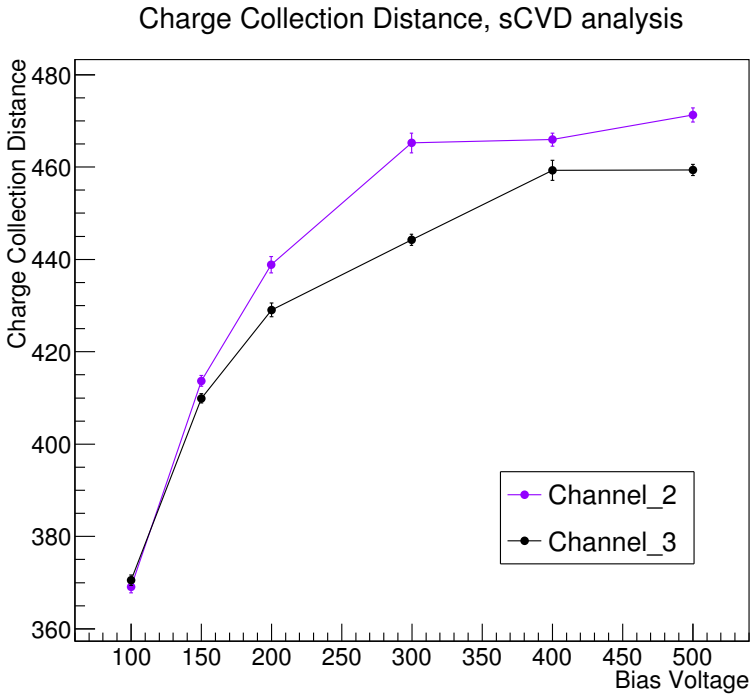

Figure 24: Charge collection distance, sCVD analysis

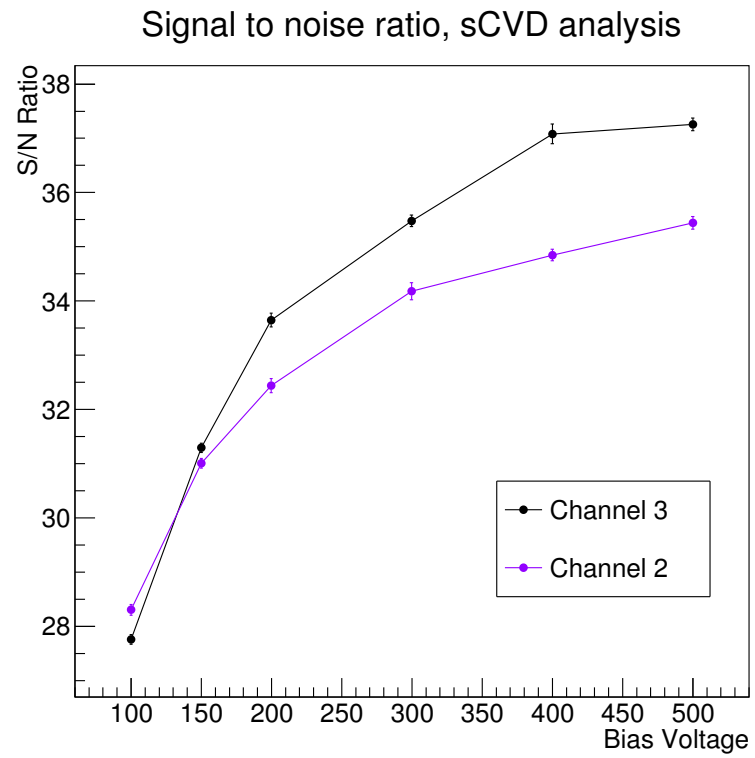

Figure 25: Singal to noise ratio, sCVD analysis

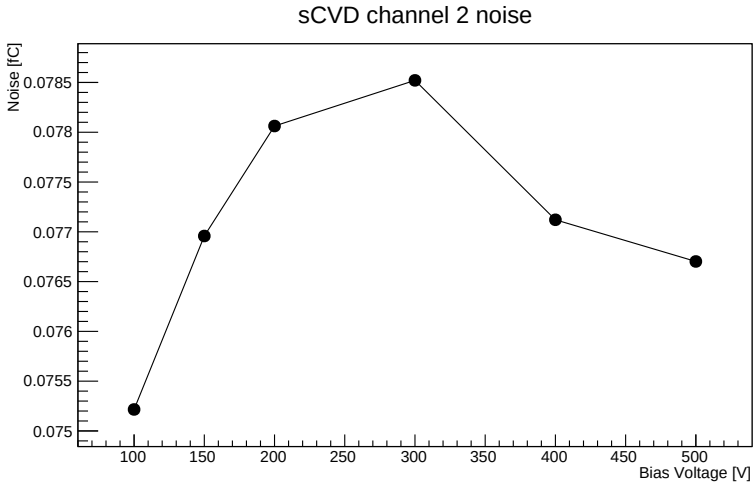

Figure 26: Noise measured for sCVD channel 2

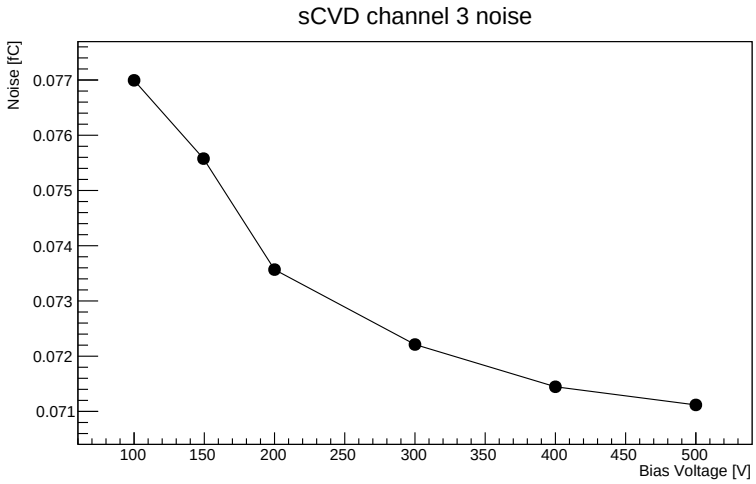

Figure 27: Noise measured for sCVD channel 3

Table 1: Charge collection distance and signal to noise ratio values calculated for all sCVD configurations

Channel	Bias voltage[V]	CCD[μm]	S/N ratio
2	100	369	28.3
2	150	414	31
2	200	439	32.4
2	300	465	34.2
2	400	466	34.9
2	500	471	35.4
3	100	371	27.8
3	150	410	31.3
3	200	429	33.6
3	300	444	35.5
3	400	459	37.1
3	500	459	37.3

Table 2: Charge collection distance and signal to noise ratio values calculated for best pCVD configurations

Configuration	CCD[μm]	S/N ratio
Neg900V RD42 resistors	120	12
Pos1000V pumped overnight	145	12
Pos1000V RD42 resistors	105	11
pCVD91 1000V v2	83	7
pCVD91 1000V	104	9

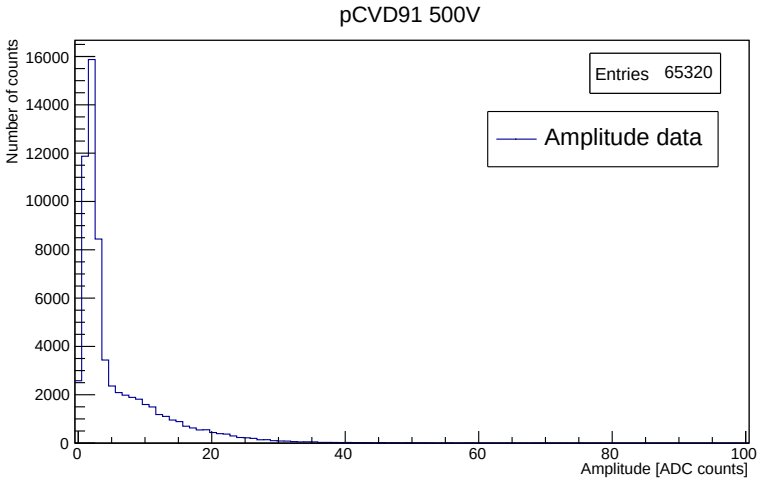

Figure 28: Amplitude distribution of data taken from pCVD91 500V configuration

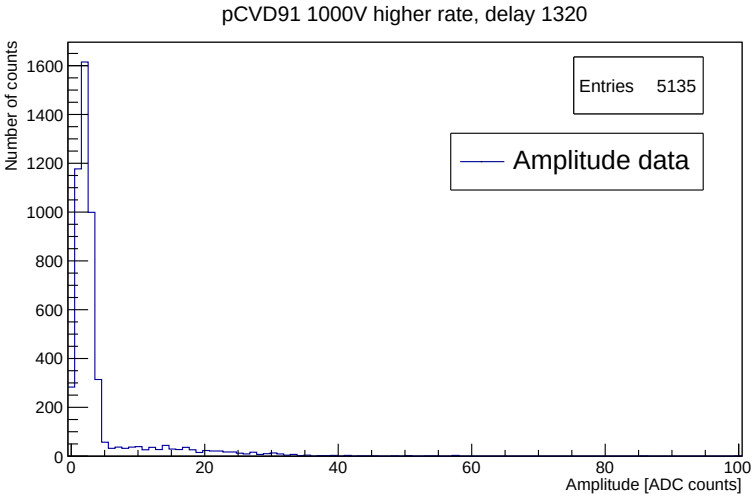

Figure 29: Amplitude distribution of data taken from pCVD 1000V

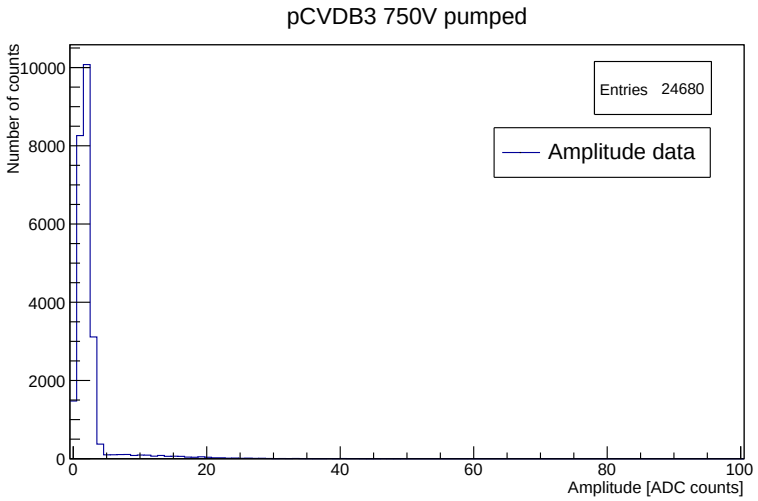

Figure 30: Amplitude distribution of data taken from pCVDB3 750V pumped configuration

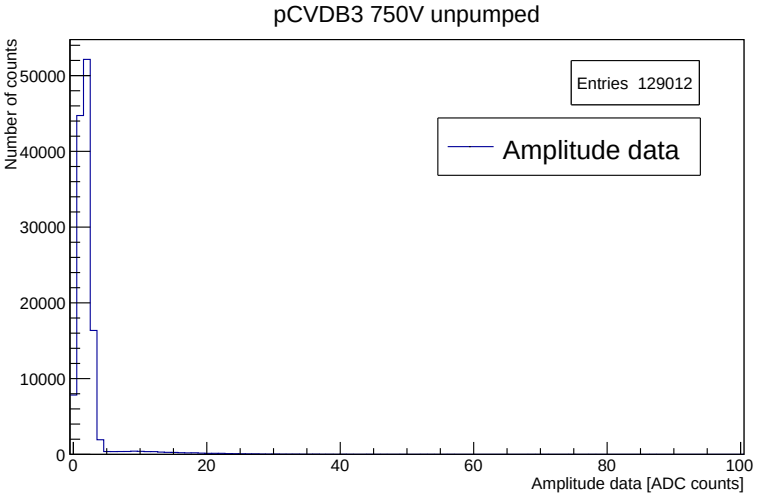

Figure 31: Amplitude distribution of data taken from pCVDB3 750V unpumped configuration

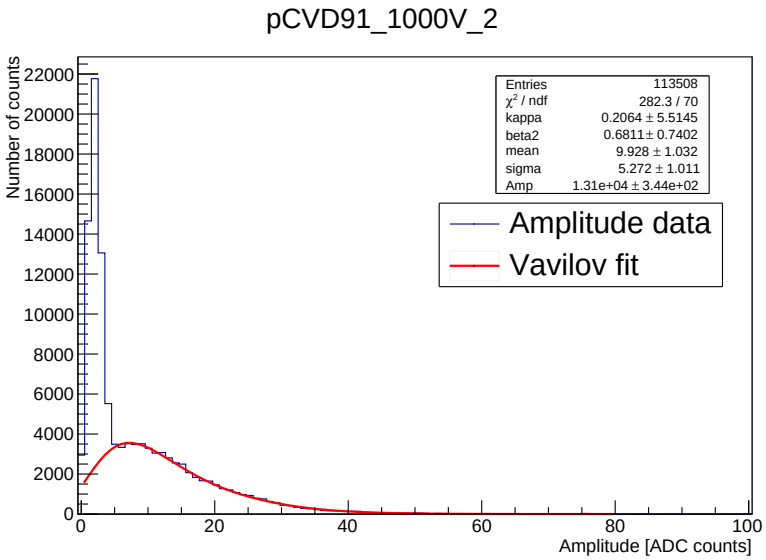

Figure 32: Amplitude distribution of data taken from pCVD91 1000V v2 configuration

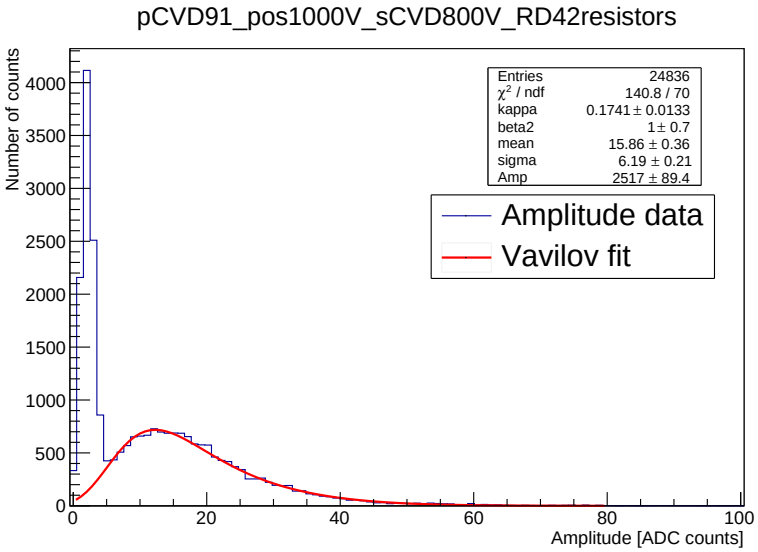

Figure 33: Amplitude distribution of data taken from pCVD91 pos1000V RD42 configuration

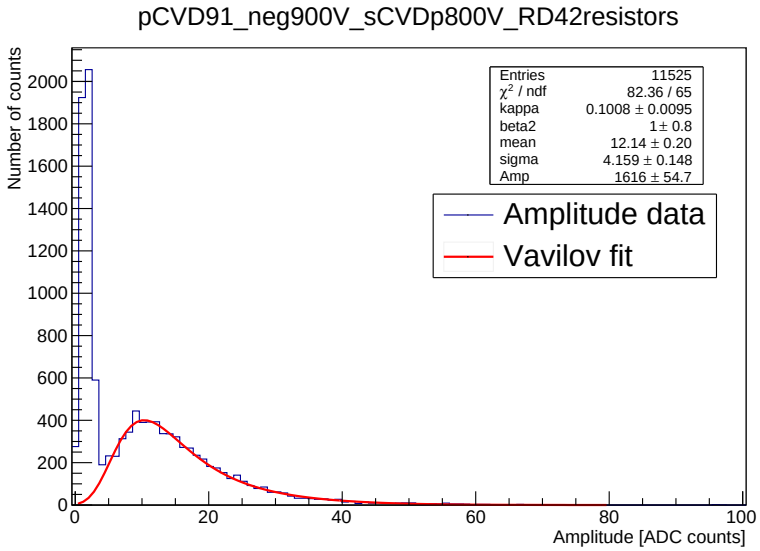

Figure 34: Amplitude distribution of data taken from pCVD91 neg900V RD42 configuration

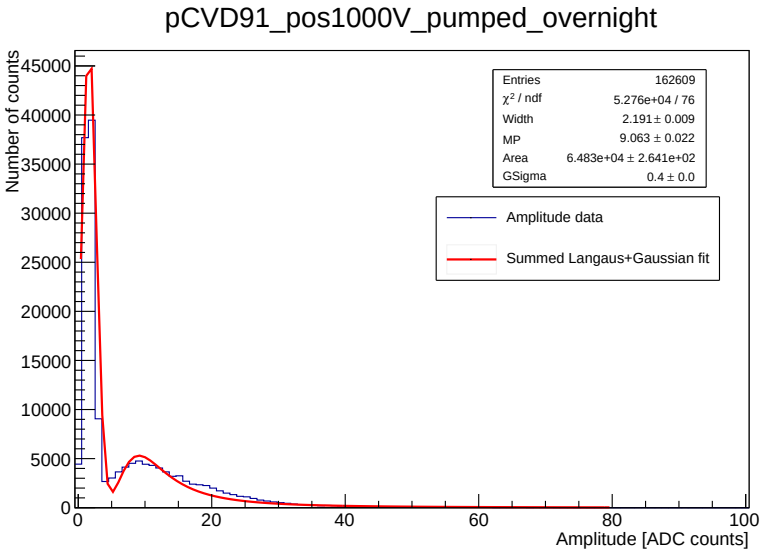

Figure 35: Amplitude distribution of data taken from pCVD91 pos1000V pumped overnight configuration

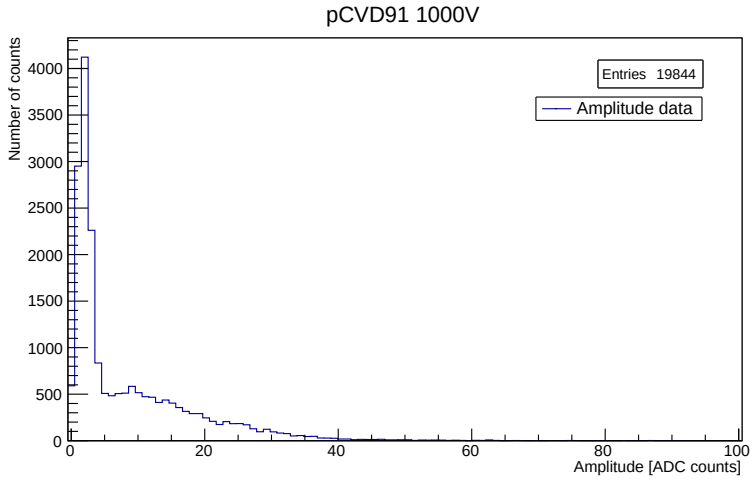

Figure 36: Amplitude distribution of data taken from pCVD91 1000V configuration

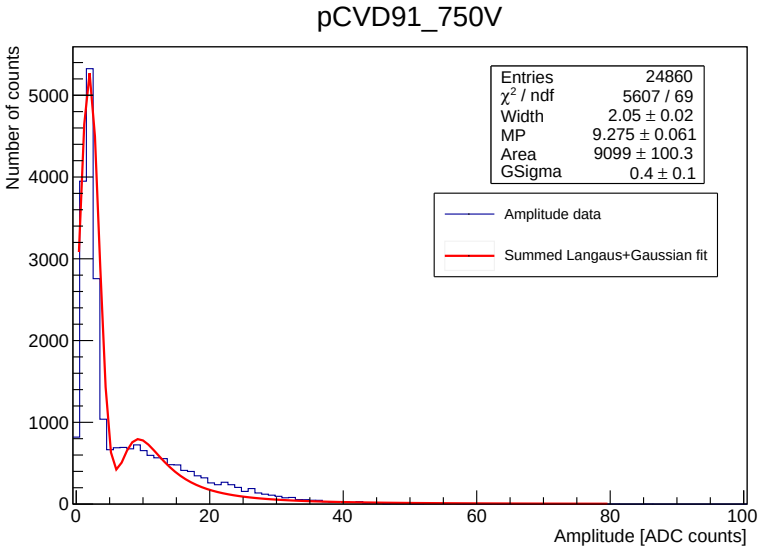

Figure 37: Amplitude distribution of data taken from pCVD91 750V configuration

6 Conclusions

Efficiency analysis of sensors currently mounted in BCM1F detector leads to need to sensors exchange in the near future. Observed evolution of polarization effect needs to be more investigated. Polycrystalline diamond sensors show at least 3 times worse performance than single crystalline ones, but they expected to be more radiation hard. That feature may allow pCVD diamonds to survive longer in terms of efficiency, which is very desirable due to planned LHC improvements. For future sensors analysis it would be useful to perform noise measurements without beam.

References

[1] A. Bell, E. Castro, R. Hall-Wilton, W. Lange, W. Lohmann, A. Macpherson, M. Ohlerich, N. Rodriguez, V. Ryjov, R.S. Schmidt, and R.L. Stone. Fast beam conditions monitor {BCM1F} for the {CMS} experiment. *Nuclear Instruments and Methods in Physics Research Section A: Accelerators, Spectrometers, Detectors and Associated Equipment*, 614(3):433 – 438, 2010.

[2] M. Hempel, K. Afanaciev, P. Burtowy, A. Dabrowski, H. Henschel, M. Idzik, O. Karacheban, W. Lange, J. Leonard, I. Levy, W. Lohmann, B. Pollak, D. Przyborowski, V. Ryjov, S. Schuwalow, D. Stickland, R. Walsh, and A. Zagozdzinska. Measurements of the performance of a beam condition monitor prototype in a 5 gev electron beam. *Nuclear Instruments and Methods in Physics Research Section A: Accelerators, Spectrometers, Detectors and Associated Equipment*, 826:65 – 71, 2016.

[3] R J Tapper. Diamond detectors in particle physics. *Reports on Progress in Physics*, 63(8):1273, 2000.

[4] S. van der Meer. Calibration of the Effective Beam Height in the ISR. 1968.

[5] A.A. Zagozdzinska, A.J. Bell, A.E. Dabrowski, M. Hempel, H.M. Henschel, O. Karacheban, D. Przyborowski, J.L. Leonard, M. Penno, K.T. Pozniak, M. Miraglia, W. Lange, W. Lohmann, V. Ryjov, A. Lokhovitskiy, D. Stickland, and R. Walsh. New fast beam conditions monitoring (bcm1f) system for cms. *Journal of Instrumentation*, 11(01):C01088, 2016.